1st Pan-American Congress on Computational Mechanics - PANACM 2015
XI Argentine Congress on Computational Mechanics - MECOM 2015
S. Idelsohn, V. Sonzogni, A. Coutinho, M. Cruchaga, A. Lew & M. Cerrolaza (Eds)

CONTINUOUS MICROPLANE THEORY AND INTERFACE APPROACH FOR FAILURE FORM ANALYSIS OF STEEL FIBER REINFORCED CONCRETE

SONIA M. VRECH[1], ANTONIO CAGGIANO[2] AND GUILLERMO ETSE[1,2]

[1]CONICET - University of Tucumán
Av. Independencia 1800. 4000 - San Miguel de Tucumán. Argentina
svrech@herrera.unt.edu.ar

[2]CONICET - University of Buenos Aires
Av. Las Heras 2214 - C1127AAR - Buenos Aires. Argentina
acaggiano@fi.uba.ar
getse@herrera.unt.edu.ar

Key words: Discontinuous bifurcation, microplanes, SFRC, interfaces, fracture

Abstract. A fracture energy-based microplane constitutive theory for steel fiber reinforced concrete (SFRC) is presented to evaluate the properties of the discontinuous bifurcation condition under different scenarios of stress states, fiber contents and directions. The constitutive model considers a CAP-cone yield surface of C^1 continuity at the microplane level. Its evolution in the post-peak regime is described by means of a fracture energy-based work softening which is defined differently for mode I and II type of failure. The effect on the post-peak ductility introduced by the fiber content is also taken into account, while the directional properties of the steel fibers are considered through the relative directions between microplanes and fibers.

The main objective of the discontinuous bifurcation analysis proposed in this work, is to evaluate the capabilities of the microplane theory to capture the directional enrichment provided by steel fibers to the ductility and also, to reproduce the particular microcrack directions which (in the framework of the smeared crack approach) are mathematically represented by the spectral properties of the critical localization tensor. Firstly, the localized failure features in the form of discontinuous bifurcation of SFRC are identified by means of numerical analysis. Mono- and multidirectional fiber distributions and different steel fiber contents are considered in the localized failure analysis to be performed on stress states corresponding to critical strengths of SFRC under both uniaxial and biaxial tension and compression. Then, microplane model are compared with the FE predictions obtained with the interface model for FRC previously proposed by the authors. In the last case, the crack evolutions and their directions are explicitly described throughout the so-called discrete crack approach.

1 INTRODUCTION

Localized failure mechanisms on quasi-brittle materials, understood as the formation of restricted failure zones with high concentration of deformations while the rest of the structure might even exhibit unloading, depend on their acting stresses as well as the mechanical and chemical features which they are submitted and have experimentally been observed by a. o. [1, 2].

While the localization of deformations in terms of discontinuous bifurcation for plain concrete has extensively been studied, see a.o. [3, 4], there are not yet similar analysis related to fiber reinforced concrete (FRC). In this case it becomes necessary to distinguish failure mechanisms that characterize tension, compression and shear regimes regarding different fiber contents as well as fiber directions.

In this work, a novel constitutive formulation for SFRC is formulated in the framework of the Mixture Theory by [5] and based on the microplane model. At microplanes level, it is described in terms of normal and shear stresses and their related strains. An hyperbolic yield surface has been adopted while a CAP-cone one of C^1 continuity describes the constitutive behavior in the high confinement regime. Their evolution in the post-peak regime is described by means of a fracture energy-based work softening which is defined differently for mode I and II type of failure. Fiber effect on the composite failure behavior is taken into account through both a bond-slip formulation and a dowel model depending on the relative orientations between fibers and microplanes.

Then, the capabilities of the microplane theory to capture the directional enrichment provided by steel fibers to the ductility and to reproduce the particular microcrack directions are evaluate and compared against FE predictions performed by the authors in the framework of the discrete approach [6].

The thermodynamically consistent microplane-based elasto-platicity theory is summarized in Section 2 while the analytical solution for localized failure in terms of discontinuous bifurcation is developed in Section 3. Then, in Section 4 the adopted composite constitutive formulation for SFRC is described. Finally, Section 5 shows the localized failure analysis for SFRC and later, the concluding remarks are highlighted in Section 6.

2 THERMODYNAMICALLY CONSISTENT MICROPLANE-BASED ELASTO-PLATICITY

The thermodynamically consistent microplane-based elasto-platicity theory for the derivation of macroscopic stresses and equilibrium equations in the case of isotropic plasticity have been developed by [7] and [8].

Assuming kinematic constraints, scalar volumetric strain and tangential strain vector at microplane level (ε_V and $\boldsymbol{\varepsilon}_T$, respectively) are computed by means of the following relationships

$$\varepsilon_V = \boldsymbol{V} : \boldsymbol{\varepsilon} \quad , \quad \boldsymbol{\varepsilon}_T = \boldsymbol{T} : \boldsymbol{\varepsilon} \tag{1}$$

being $\boldsymbol{\varepsilon}$ the macroscopic strain tensor projected on a microplane of normal direction $\boldsymbol{n}$. The projection tensors are defined as

$$\boldsymbol{V} = \frac{1}{3}\boldsymbol{I} \quad , \quad \boldsymbol{T} = \boldsymbol{n} \cdot I^{sym} - \boldsymbol{n} \otimes \boldsymbol{n} \otimes \boldsymbol{n} \tag{2}$$

being I^{sym} the symmetric part of the fourth-order identity tensor.

Thus, the strain vector at microplane level results

$$\boldsymbol{t}_\varepsilon = \varepsilon_V \boldsymbol{n} + \boldsymbol{\varepsilon}_T. \tag{3}$$

Assuming the macro free-energy potential as the integral of the micro free-energy on a spherical region of unit volume Ω, the following micro-macro free-energy relationship is proposed

$$\psi^{mac} = \frac{3}{4\pi} \int_\Omega \psi^{mic} \mathrm{d}\Omega \tag{4}$$

being $\psi^{mic}{=}\psi^{mic}(\varepsilon_V, \boldsymbol{\varepsilon}_T, \kappa)$ the free-energy potential at microplane level, expressed in terms of the strain components and the scalar internal variable κ. Assuming small strains and considering the additive decomposition into elastic and plastic parts of the macroscopic strain tensor, the microscopic strain components are expressed as

$$\varepsilon_V = \varepsilon_V^e + \varepsilon_V^p \quad , \quad \boldsymbol{\varepsilon}_T = \boldsymbol{\varepsilon}_T^e + \boldsymbol{\varepsilon}_T^p. \tag{5}$$

Then, the constitutive micro-stresses and their rates are computed as

$$\begin{aligned} \sigma_V &= \frac{\partial \psi^{mic}}{\partial \varepsilon_V} \quad \rightarrow \quad \dot{\sigma}_V = E_V^e[\dot{\varepsilon}_V - \dot{\varepsilon}_V^p] \\ \boldsymbol{\sigma}_T &= \frac{\partial \psi^{mic}}{\partial \boldsymbol{\varepsilon_T}} \quad \rightarrow \quad \dot{\boldsymbol{\sigma}}_T = E_T^e[\dot{\boldsymbol{\varepsilon}}_T - \dot{\boldsymbol{\varepsilon}}_T^p] \end{aligned} \tag{6}$$

while the dissipative stresses and their rates can be computed at microplane level as

$$\phi^{mic} = \frac{\partial \psi^{mic}}{\partial \kappa} \quad \rightarrow \quad \dot{\phi}^{mic} = \bar{H}\dot{\kappa} \tag{7}$$

being $\bar{H}$ the hardening/softening modulus.

As in case of macroscopic plasticity, both yield and plastic potential surfaces are set as

$$\begin{aligned} &\Phi^{mic}(\sigma_V, \boldsymbol{\sigma}_T, \phi^{mic}) \leq 0 \quad \text{with} \quad \nu_V = \frac{\partial \Phi^{mic}}{\partial \sigma_V} \quad \text{and} \quad \boldsymbol{\nu}_T = \frac{\partial \Phi^{mic}}{\partial \boldsymbol{\sigma}_T} \\ &\Phi^{*mic}(\sigma_V, \boldsymbol{\sigma}_T, \phi^{mic}) \leq 0 \quad \text{with} \quad \mu_V = \frac{\partial \Phi^{*mic}}{\partial \sigma_V} \quad \text{and} \quad \boldsymbol{\mu}_T = \frac{\partial \Phi^{*mic}}{\partial \boldsymbol{\sigma}_T} \end{aligned} \tag{8}$$

and the evolution of the plastic strain components yields

$$\dot{\varepsilon}_V^p = \dot{\lambda}\mu_V \quad , \quad \dot{\boldsymbol{\varepsilon}}_T^p = \dot{\lambda}\boldsymbol{\mu}_T \quad , \quad \dot{\kappa} = \dot{\lambda}. \tag{9}$$

Moreover, the Kuhn-Tucker and consistency conditions must be satisfied

$$\Phi^{mic} \leq 0 \quad , \quad \dot{\lambda} \geq 0 \quad , \quad \Phi^{mic}\dot{\lambda} = 0 \quad \text{and} \quad \dot{\Phi}^{mic}\dot{\lambda} = 0 \tag{10}$$

The homogenization of the microplanes energy of Eq. (4) leads to the definition of the macroscopic stress tensor as

$$\boldsymbol{\sigma} = \frac{\partial \psi^{mac}}{\partial \boldsymbol{\varepsilon}} = \frac{3}{4\pi}\int_{\Omega} \boldsymbol{V}\sigma_V + \boldsymbol{T}^T \cdot \boldsymbol{\sigma}_T d\Omega. \tag{11}$$

The analytical evaluation of this integral can be solved by numerical integration techniques proposed by [9]. Thus, Eq. (11) can be rewritten as

$$\boldsymbol{\sigma} \approx \sum_{I=1}^{n_{mic}} \left[\boldsymbol{V}^I {\sigma_V}^I + \boldsymbol{T}^{TI} \cdot {\boldsymbol{\sigma_T}}^I\right] w^I \tag{12}$$

where the superscript I denotes the I_{th} material direction and w^I the corresponding weight coefficients. The number of microplanes n_{mic} that ensures accurate approximations is 42.

The macroscopic tangent operator can be analogously obtained as

$$E^{ep} = \frac{d\boldsymbol{\sigma}}{d\boldsymbol{\varepsilon}} = \frac{3}{4\pi}\int_{\Omega}\left[\boldsymbol{V} \otimes \frac{d\boldsymbol{\sigma}}{d\varepsilon_V} + \boldsymbol{T}^T \cdot \frac{d\boldsymbol{\sigma}}{d\boldsymbol{\varepsilon}_T}\right] d\Omega \tag{13}$$

resulting

$$E^{ep} = E^e - \frac{3}{4\pi}\int_{\Omega}\frac{1}{h}\left[E_V^e \boldsymbol{V}\mu_V + E_T^e \boldsymbol{T}^T \cdot \boldsymbol{\mu}_T\right] \otimes \left[\nu_V \boldsymbol{V} E_V^e + \boldsymbol{\nu}_T \cdot \boldsymbol{T}^T E_T^e\right] d\Omega \tag{14}$$

with the elastic macroscopic tangent operator computed as

$$E^e = \frac{3}{4\pi}\int_{\Omega} E_V^e \boldsymbol{V} \otimes \boldsymbol{V} + E_T^e \boldsymbol{T}^T \cdot \boldsymbol{T} d\Omega. \tag{15}$$

3 ANALYTICAL SOLUTION FOR LOCALIZED FAILURE IN MICROPLANE-BASED ELASTO-PLATICITY

In the framework of the smeared crack approach, localized failure modes are related to discontinuous bifurcations of the equilibrium path, and lead to lost of ellipticity of the equations that govern the static equilibrium problem. The inhomogeneous or localized deformation field exhibits a plane of discontinuity that can be identified by means of the eigenvalue problem of the acoustic or localization tensor, see [10].Analytical solutions for the discontinuous bifurcation condition conduce to the macroscopic localization condition

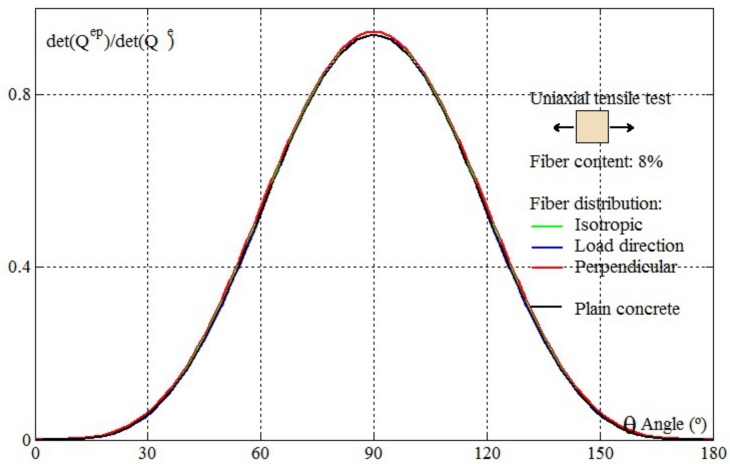

Figure 1: Numerical localization analysis with the microplane-based criterion at peak of the uniaxial tension tests of SFRC with 8 % fiber content.

$$det(\boldsymbol{Q}^{ep}) = 0. \tag{16}$$

In case of microplane-based plasticity, the acoustic tensor is expressed as

$$\boldsymbol{Q}^{ep} = \boldsymbol{Q}^{e} - \frac{3}{4\pi}\int_{\Omega} \frac{\boldsymbol{a}^{*} \otimes \boldsymbol{a}}{h} d\Omega \tag{17}$$

with the traction vectors computed as

$$\begin{aligned} \boldsymbol{a} &= [\nu_V \boldsymbol{V} E_V^e + \boldsymbol{\nu}_T \cdot \boldsymbol{T} E_T^e] \cdot \boldsymbol{n}, \\ \boldsymbol{a}^{*} &= \boldsymbol{n} \cdot [E_V^e \boldsymbol{V} \mu_V + E_T^e \boldsymbol{T} \cdot \boldsymbol{\mu}_T] \,. \end{aligned} \tag{18}$$

Analytical solutions of the acoustic tensor's eigenvalues and eigenvector problem lead to explicit solutions of critical hardening/softening modulus

$$\bar{H}_c = \boldsymbol{a} \cdot [\boldsymbol{Q}^{ep}]^{-1} \cdot \boldsymbol{a}^{*} - \boldsymbol{\nu} : \boldsymbol{E}^{e} : \boldsymbol{\mu} = 0 \tag{19}$$

as well as critical localization angles θ_i, that define the localization directions $\boldsymbol{n}$, normal to the failure surface S.

Due to the complex structure of the acoustic tensor for microplane-based plasticity in Eq. (17), the analytical assessment is not easy. Instead, numerical solutions must be applied and Eq. (17) can be rewritten as

$$\boldsymbol{Q}^{ep} \approx \boldsymbol{Q}^{e} - \sum_{I=1}^{n_{mic}} \left[\frac{\boldsymbol{a}^{*I} \otimes \boldsymbol{a}^{I}}{h^{I}} \right] w^{I}. \tag{20}$$

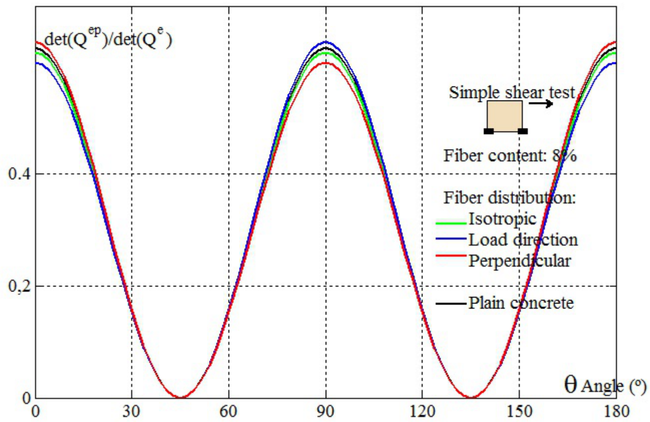

Figure 2: Numerical localization analysis with the microplane-based criterion at peak of the simple shear tests of SFRC with 8 % fiber content.

4 COMPOSITE CONSTITUTIVE FORMULATION FOR SFRC

In this section, the constitutive formulation for SFRC based on microplanes and Mixture Theories [5] is described. On this basis, each infinitesimal volume of the composite is characterized by the same amount and proportion of its constituents (mortar matrix and randomly oriented fiber reinforcements for SFRC). Consequently, the composite stress vector is defined as the weighted sum (in terms of the volume fraction) of the constituent stresses

$$\boldsymbol{t}_\sigma = w_m \boldsymbol{\sigma}^m + \sum_{f=1}^{n_f} w_f \left[\sigma\left(\varepsilon_N\right) \boldsymbol{n}_f + \tau\left(\boldsymbol{\varepsilon}_T\right) \boldsymbol{t}_f\right] \tag{21}$$

being ω_m and ω_f the weighting functions depending on the volume fraction of each constituent, with m and f indicating mortar and fiber, respectively. The mortar stress vector is computed as $\boldsymbol{\sigma}^m = [\sigma_N \;\; \boldsymbol{\sigma}_T]$; σ and τ mean the bond-slip and dowel stresses of the single fibers, related to their axial and tangential strains, ε_N and $\boldsymbol{\varepsilon}_T$; while $\boldsymbol{n}_f$ and $\boldsymbol{t}_f$ are the vectors in the fiber and its orthogonal directions, respectively.

4.1 Failure surfaces evolution for plain mortar

The maximum strength criterion of the aforementioned fracture energy-based plasticity formulation for plain mortar combines the three-parameter hyperbolic strength function by [11], in terms of the initial tensile strength χ_0, cohesion c_0 and the internal friction angle φ_0; with an elliptical CAP surface to more accurately compute mortar peak capacity in the high confinement regime. There are expressed as

$$\Phi_{hyp} = {\sigma_T}^2 - \left[c_0 - \sigma_N \tan(\varphi_0)\right]^2 + \left[c_0 - \chi_0 \tan(\varphi_0)\right]^2 \quad \text{if} \quad \sigma_{C,0} \leq \sigma_N \leq \chi_0 \tag{22}$$

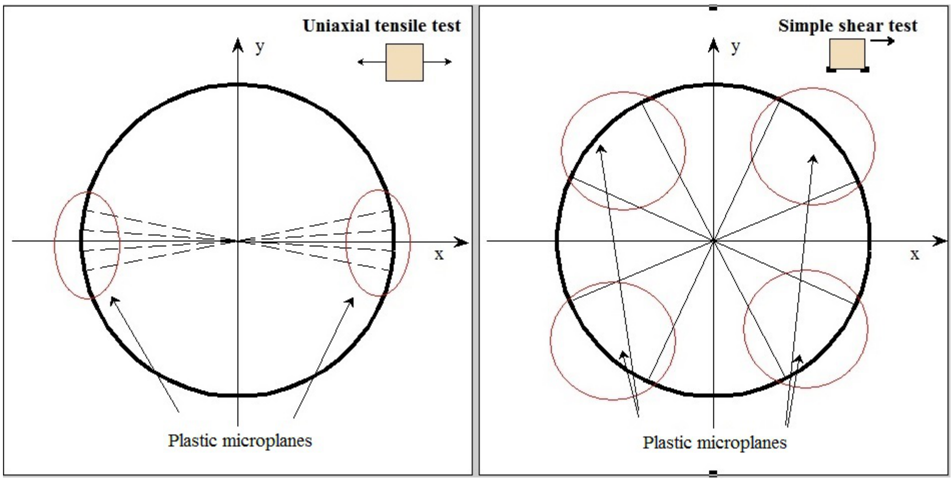

Figure 3: Plastic microplanes at peak strees of the uniaxial tensile and simple shear tests.

$$\Phi_{CAP} = {\sigma_T}^2 - \left[\frac{(\sigma_{L,0} - \sigma_{A,0})^2 - (\sigma_N - \sigma_{A,0})^2}{{\tau_0}^2} \right] = 0 \quad \text{if} \quad \sigma_N < \sigma_{C,0} \tag{23}$$

being $\sigma_T = \|\boldsymbol{\sigma}_T\|$. $\sigma_{A,0}$, $\sigma_{L,0}$ and τ_0 are material parameters of the CAP. The limit strength $\sigma_{C,0}$ corresponds to the particular value of σ_N for which the equality and continuity conditions for Φ_{hyp} and Φ_{CAP} take place.

The plastic flow rule, computed as

$$\dot{\boldsymbol{\varepsilon}}^p = \left[\begin{array}{c} \varepsilon_N^p \\ \varepsilon_T^p \end{array} \right] = \dot{\lambda} \boldsymbol{A} \cdot \left(\begin{array}{c} \nu_N \\ \nu_T \end{array} \right) \tag{24}$$

being

$$\nu_N = \frac{\partial \Phi}{\partial \sigma_N} \quad , \quad \nu_T = \frac{\partial \Phi}{\partial \sigma_T} \tag{25}$$

can be subdivided in five zones according to the confinement level, characterized by particular expressions of the matrix $\boldsymbol{A}$.

The post-cracking behavior is controlled by the rate of the plastic work spent, named $\dot{w}$, during three possible post-peak failure mechanisms: mode I, shear or mode II and pure compaction.

For the sake of brevity, the complete description of the models are omitted. Further details can be found in [12].

4.2 Failure surfaces evolution for steel fibers

Steel fiber actions, developed on active opened cracks, offer bridging effects on the overall SFRC post-peak behavior. On the one hand, the bond-slip mechanism between fibers

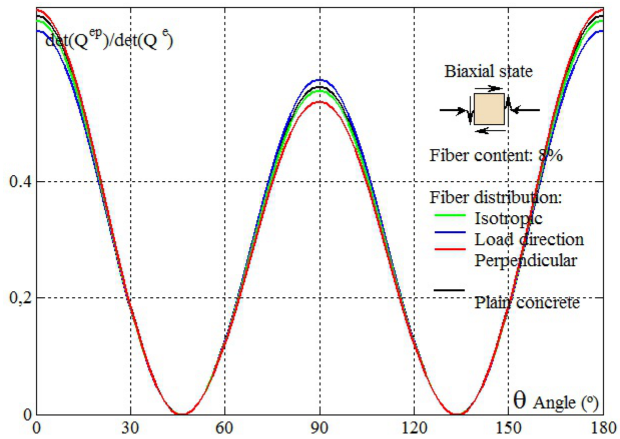

Figure 4: Numerical localization analysis with the microplane-based criterion at peak of the biaxial tests of SFRC with 8 % fiber content.

and concrete matrix is treated as an axial (tensile) fiber stress acting at microplane level. On the other hand, a dowel effect is considered to model the shear transfer mechanism which develops in case of fibers crossing active cracks while they are subjected to stresses in the normal direction to fibers.

The complete formulations of both, the bond-slip and dowel action, have been detailed in [12].

5 SOLUTION FOR DISCONTINUOUS BIFURCATION ANALYSIS OF SFRC

In this section, numerical localization analysis of SFRC have been performed regarding the microplane-based formulation developed in previous sections. Based on the 2D formulation of the microplane-based elasto-plasticity by [13], 48 microplanes have been considered for the integration of stresses at each material point. Plane strain state has been considered, regarding the particular condition when $\sigma_z = \nu(\sigma_x + \sigma_y)$.

The evaluation of localization conditions signalized by the appearance of null values of the normalized determinant of the acoustic tensor corresponding to discontinuous bifurcation [$\det(Q^{ep})/\det(Q^e)$=0], has been carried out at the peak stresses corresponding to the simple shear, uniaxial tensile, uniaxial compression and biaxial tests.

The model parameters are adjusted according the experimental data given by [14], being $E_c = 39.5\,GPa$ and $\nu = 0.20$, $\tan(\varphi_0) = 0.6$, $\chi_0 = 4.0\,MPa$, $c_0 = 7.0\,MPa$, $\sigma_{C,0} = -7.0\,MPa$, $\tau_0 = 0.25$, $G_f^I = 0.12\,N/mm$ and $G_f^{IIa} = 1.2\,N/mm$. While, those corresponding with the fiber-concrete interactions are: $E_s = 200.0\,GPa$, $\nu = 0.30$, $\sigma_{y,s} = 1.2\,MPa$ and $\tau_{y,f} = 2.35\,MPa$.

As can be observed in Figs. (1) and (2), in case of the uniaxial tensile and the simple shear tests, failure conditions are fulfilled in the critical directions θ= 0° - 180° and θ=45°

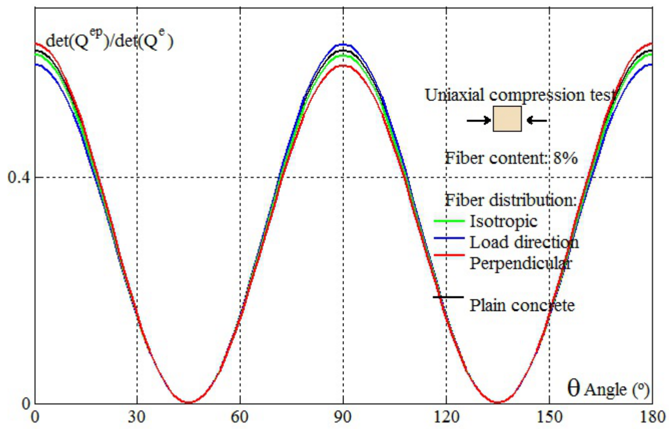

Figure 5: Numerical localization analysis with the microplane-based criterion at peak of the uniaxial compression tests of SFRC with 8 % fiber content.

- 135°, respectively, agreeing for all fiber directions. Figure (3) indicates the position of plastic microplanes for the both cases. In the first case, it corresponds to microplanes located between 0° and 15° on each hemisphere and in the second case, to those between 30° and 80°.

Under biaxial and uniaxial compression tests, the localized failure condition is also fulfilled. Regarding Figs. (4) and (5), the numerical localization condition is achieved at θ= 48° - 132° and θ=45° - 135°, respectively. Plastic microplanes are located at 30° and at 85° in the case of biaxial test, whereas in the case of uniaxial compression, between 0° and 15° in each hemisphere, see Fig. (6).

The sensitivity of the failure behaviour based on the microplane theory regarding the orientation of fibers in the cementitious matrix has been evaluated. To this end, four different fiber contents, 0, 3, 8 and 20% (theoretical case) with isiotropical distribution have been considered in the uniaxial tensile test. The results in terms of numerical localization analysis are shown in Fig. (7). It can be observed, critical localization directions remain unchanged with increasing fiber contents.

Finally, the capabilities of the microplane theory to reproduce the particular microcrack directions are compared against FE predictions performed by the authors [12, 6] in the frame work of the discrete approach, with the mesoscale interface model for SFRC.

The following examples serve to validate the results obtained in this section. The case of SFRC three-point bending problem with centrical notch by [15] is considered. Crack paths in tensile region reproduces a localization angle perpendicular to the load direction, see Fig. (8). In second place, the shear tests on SFRC specimens is evaluated. As can be observed in Fig. (9), a critical localization direction at 45° is reproduced.

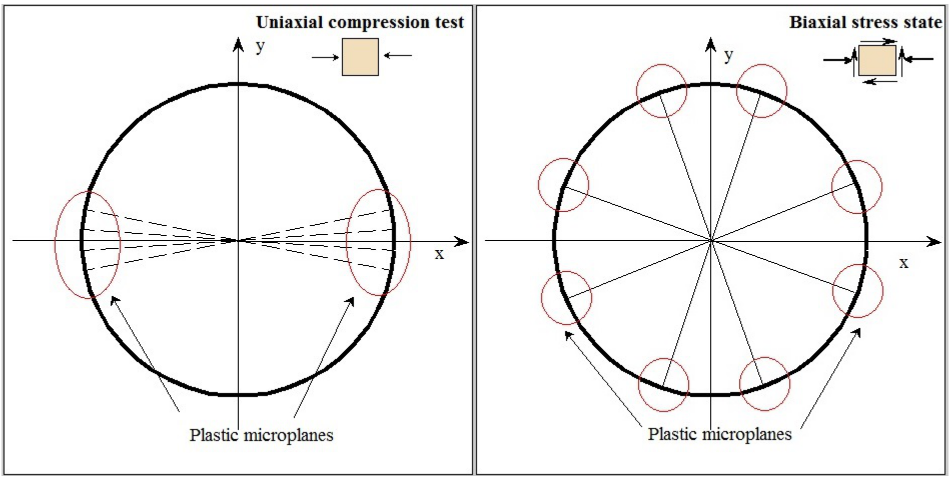

Figure 6: Plastic microplanes at peak strees of the uniaxial compression and biaxial tests.

6 CONCLUSIONS

In this work, an elasto-plastic microplane constitutive model aimed at predicting the failure behavior of steel fiber reinforced Concrete (SFRC) has been described. The constitutive formulation considers the well-known Mixture Theory to simulate the combined bridging interactions of fibers in concrete cracks, i.e. fiber-to-concrete bond-slip as well as dowel mechanisms.

Numerical analysis of the condition for discontinuous bifurcation, based on the evaluation of the spectral properties of the acoustic or localization tensor through the calculation of its determinant, has been applied.

The obtained results for the localization analysis under plane strain conditions demonstrate the capabilities of the constitutive model for concrete to reproduce localized failure. The numerical results also demonstrate the capabilities of the proposed constitutive theory to capture the directional orientation of the steel fiber reinforcements embedded in the cementitious matrix.

REFERENCES

[1] Petersson, P.E. *Crack growth and development of fracture zones in plain concrete and similar materials*. Report TVBM-1006. Technical report, Lund Institute of Technology, Sweden, (1981).

[2] van Mier, J.G.M. *Fracture processes of concrete*. CRC Press, (1997).

[3] Rudnicki, J. and Rice, J. Conditions for the localization of deformation in pressure-sensitive dilatant materials. *J. Mech. Phys. Solids* (1975) **23**: 371–394.

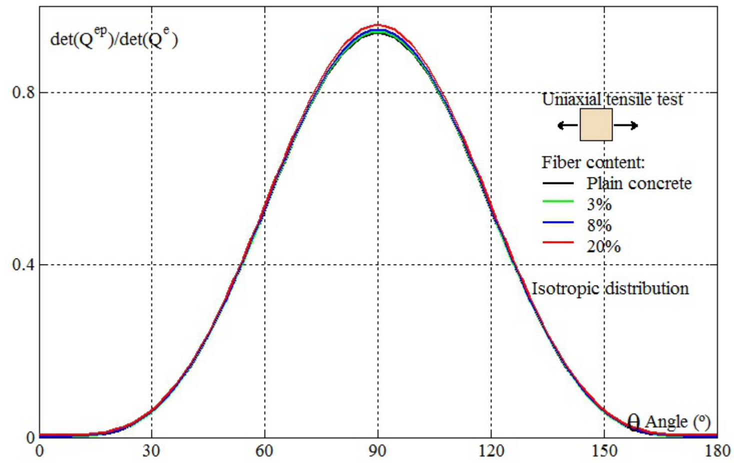

Figure 7: Numerical localization analysis with the microplane-based criterion at peak of the uniaxial tension tests of SFRC with variable fiber contents: 0, 3, 8 and 20%.

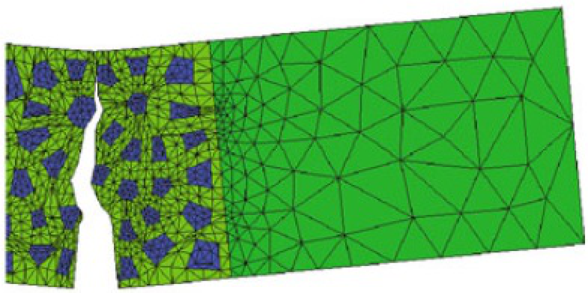

Figure 8: SFRC three-point bending problem with centrical notch by [15], reproduced by [6].

[4] Perić, D. *Localized deformation and failure analysis of pressure sensitive granular materials*. University of Colorado, CEAE Dept., Boulder, USA. (1990).

[5] Truesdell, C. and Toupin, R. *The classical field theories. Handbuch der Physik*. Springer-Verlag, Berlin III/I. (1960).

[6] Etse, G. and Caggiano, A. and Vrech, S. Multiscale failure analysis of fiber reinforced concrete based on a discrete crack model. *Int. J. of Fracture* (2012) **178 (1-2)**: 131–146.

[7] Carol, I. and Jirasek, M. and Bažant, Z. A thermodynamically consistent approach to microplane theory. Part I. Free-energy and consistent microplane stresses. *Int. J. of Solids and Struct.* (2001) **38(17)**: 2921–2931.

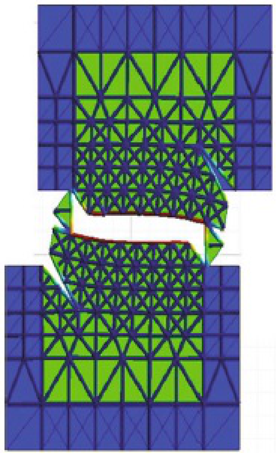

Figure 9: Shear tests on SFRC, reproduced by [6].

[8] Kuhl, E. and Steinmann, P. and Carol, I. A thermodynamically consistent approach to microplane theory. Part II. Dissipation and inelastic constitutive modeling, *Int. J. of Solids and Struct.* (2001) **38(17)**: 2933–2952.

[9] Bažant, Z. and Oh, B. Efficient numerical integration on the surface of a sphere. *ZAMM*, (1986) **66**: 37–49.

[10] Ottosen, S. and Runesson, K. Properties of discontinuous bifurcation solutions in elasto–plasticity. *Int. J. of Solids and Structures* (1991) **27**: 401–421.

[11] Carol, I. and Prat, P. C. and Lopez, C. M. Normal/shear cracking model: Applications to discrete crack analysis. J. of Engrg. Mechanics (1997) **123**: 765–773.

[12] Caggiano, A. and Etse, G. and Martinelli, E. Zero-thickness interface model formulation for failure behavior of fiber-reinforced cementitious composites. *Computers and Structures* (2012) **98-99**: 23–32.

[13] Park, H. and Kim, H. Microplane Model for Reinforced-Concrete Planar Members in Tension-Compression. *J. of Struct. Eng, ASCE* (2003) **337**: 337–345.

[14] Li, F. and Li, Z. Continuum damage mechanics based modeling of fiber reinforced concrete in tension. *Int. J. of Solids and Structures* (2001) **38-5**: 777–793.

[15] Carpinteri, A. and Brighenti, R. Fracture behaviour of plain and fiber-reinforced concrete with different water content under mixed mode loading. *Mater. Design* (2010) **31(4)**:2032-2042.